Cell Reports
Article

Optogenetic Mapping of Cerebellar Inhibitory Circuitry Reveals Spatially Biased Coordination of Interneurons via Electrical Synapses

Jinsook Kim,[1,2,3,4,5] Soojung Lee,[2,3,6,7] Sachiko Tsuda,[1,2,3,4,5] Xuying Zhang,[8] Brent Asrican,[8] Bernd Gloss,[8] Guoping Feng,[8,9] and George J. Augustine[1,2,3,4,5,6,10,*]
[1]Lee Kong Chian School of Medicine, Nanyang Technological University, 50 Nanyang Drive, Research Techno Plaza, Singapore 637553, Singapore
[2]Laboratory of Synaptic Circuitry, Program in Neuroscience and Behavioral Disorders, Duke-NUS Graduate Medical School, 8 College Road, Singapore 169857, Singapore
[3]A*STAR/Duke-NUS Neuroscience Research Partnership, 61 Biopolis Drive, Proteos, Singapore 138673, Singapore
[4]Institute of Molecular and Cell Biology, 61 Biopolis Drive, Proteos, Singapore 138673, Singapore
[5]Marine Biological Laboratory, Woods Hole, MA 02543, USA
[6]Center for Functional Connectomics, Korea Institute of Science and Technology, 39-1 Hawolgokdong, Seongbukgu, Seoul 136-791, Republic of Korea
[7]Department of Maxillofacial Tissue Regeneration, School of Dentistry, Kyung Hee University, Seoul 130-050, Republic of Korea
[8]Department of Neurobiology, Duke University Medical Center, Durham, NC 27710, USA
[9]McGovern Institute for Brain Research, Department of Brain and Cognitive Sciences, Massachusetts Institute of Technology, Cambridge, MA 02139, USA
[10]Department of Physiology, Yong Loo Lin School of Medicine, National University of Singapore, Singapore 117599, Singapore
*Correspondence: georgea@neuro.duke.edu
http://dx.doi.org/10.1016/j.celrep.2014.04.047

SUMMARY

We used high-speed optogenetic mapping technology to examine the spatial organization of local inhibitory circuits formed by cerebellar interneurons. Transgenic mice expressing channelrhodopsin-2 exclusively in molecular layer interneurons allowed us to focally photostimulate these neurons, while measuring resulting responses in postsynaptic Purkinje cells. This approach revealed that interneurons converge upon Purkinje cells over a broad area and that at least seven interneurons form functional synapses with a single Purkinje cell. The number of converging interneurons was reduced by treatment with gap junction blockers, revealing that electrical synapses between interneurons contribute substantially to the spatial convergence. Remarkably, gap junction blockers affected convergence in sagittal slices, but not in coronal slices, indicating a sagittal bias in electrical coupling between interneurons. We conclude that electrical synapse networks spatially coordinate interneurons in the cerebellum and may also serve this function in other brain regions.

INTRODUCTION

γ-Aminobutyric acid (GABA)ergic interneurons located in the molecular layer provide inhibitory inputs to Purkinje cells (PCs), the sole output neurons of the cerebellar cortex (Eccles et al., 1967; Palay and Chan-Palay, 1974). Molecular layer interneurons (MLIs) traditionally are divided into two types, basket and stellate cells, although these may be a single type of neuron that differ in their target location: stellate cells innervating PC dendrites and basket cells innervating PC somata and forming "pinceau" structures at the PC axon initial segment (King et al., 1993; Sultan and Bower, 1998; Bower, 2010).

MLIs cause lateral inhibition via sagittal extensions of their axons (Palay and Chan-Palay, 1974). This lateral inhibition is thought to play an important role in coordination of motor behavior by shaping the temporal and spatial pattern of PC activation (Cohen and Yarom, 2000; Dunbar et al., 2004; Gao et al., 2006). The actions of MLIs can also provide feedforward inhibition (Mittmann et al., 2005) that regulates PC activation in response to granule cell input (Gao et al., 2006; Santamaria et al., 2007; Bower, 2010; Dizon and Khodakhah, 2011).

The functional organization of the circuits formed by MLIs is not clear. MLIs outnumber PCs by a factor of ten, suggesting a high degree of convergence (Korbo et al., 1993). Anatomical studies indicate that a single PC is contacted by three to seven basket cell axons, though only one to two of these form synapses within the pinceau structure (Palay and Chan-Palay, 1974; Somogyi and Hámori, 1976). In addition, MLIs are often connected to each other through chemical and/or electrical synapses that could influence information flow between MLIs and PCs (Mann-Metzer and Yarom, 1999; Mittmann et al., 2005; Alcami and Marty, 2013). Although traditional electrophysiological recordings can reveal the function of each of these connections, such measurements provide limited information about the spatial organization of these circuits. As a result, it remains

unclear precisely how many MLIs functionally converge upon a postsynaptic PC and how this convergence is spatially organized within the molecular layer.

Here, we have visualized the functional organization of these inhibitory circuits by an optimized optogenetic mapping technique (Wang et al., 2007; Petreanu et al., 2007). With this approach, we could quantify the spatial range and degree of convergence between MLIs and PCs. We also identified a role for electrical synapses in organizing MLIs into spatially structured clusters that amplify the degree of convergence between MLIs and PCs and thereby increase the amount of lateral and feedforward inhibition. Remarkably, these clusters are spatially biased and are oriented in the sagittal plane. These findings provide features for future computational models of these local circuits (Medina and Mauk, 2000; Santamaria et al., 2007) and suggest a general role for electrical synapses in spatial coordination of interneurons.

RESULTS

Selective Expression of Channelrhodopsin in Cerebellar Interneurons

To selectively photostimulate MLIs, we engineered bacterial artificial chromosome (BAC) transgenic mice expressing channelrhodopsin-2 (ChR2; Zhao et al., 2011) under the control of the neuronal nitric oxide synthase (nNOS) promoter (Figure S1A). These transgenic mice were viable and had no obvious anatomical or behavioral deficits. To determine the location of ChR2 expression, we imaged yellow fluorescent protein (YFP) fused to the ChR2 (Figure S1B). There was high expression of ChR2-YFP in the molecular layer of the cerebellum, but not in the granule cell layer (Figure S1C). At higher magnification, ChR2-YFP was evident in the plasma membrane of somata of individual MLIs (Figure S1D, arrows) and was prominent in both axonal pericellular baskets around PC somas (Figure S1D) and pinceau terminals that envelop the axon hillock of PCs (Figure S1D, arrowheads).

Within the cerebellar cortex, both MLIs and PCs were labeled by antibodies directed against GAD67, a marker for GABAergic neurons (Figures S1E–S1G). GAD67-positive MLIs were readily identified by their smaller cell bodies and their location within the molecular layer. At postnatal day 31 (P31), 87.2% ± 1.9% (n = 3) of MLIs exhibiting cytoplasmic GAD67 staining also were positive for ChR2-YFP, and a similar value (88.7%; n = 1) was determined in an adult (P150) mouse. Conversely, ChR2-YFP was never observed in the PCs.

To examine whether the ChR2-YFP was functional, we made electrophysiological recordings from 52 MLIs in cerebellar slices from transgenic mice (P23–P33). Among these MLIs, 45 fired action potentials in response to the light spots used in our optogenetic circuit-mapping experiments (see below). This corresponds to 87% photostimulation efficacy and matches the 87%–89% of MLIs expressing ChR2 determined from histology. There was no difference between the electrical properties of ChR2-positive and ChR2-negative MLIs (Table S1). We also made recordings from five granule cells and found that even light spots 10-fold brighter than those used for mapping (see below) did not evoke action potentials in these cells (see also Heiney et al., 2014). Thus, ChR2 was preferentially expressed in the MLIs of these mice, and this allowed us to exclusively photostimulate MLIs.

Photostimulation of Cerebellar Interneurons

We further assessed optogenetic control of MLIs by illuminating sagittal cerebellar slices over a broad area (~0.23 mm^2) while recording MLI responses. Illumination (465–495 nm) reliably evoked action potentials in MLIs from mice 2–4 weeks old or older (Figure 1A), due to light-induced currents associated with ChR2 activation (Figure S2A; Wang et al., 2007). Increasing light intensity increased action potential frequency (Figure 1A), with half-maximal responses observed at a luminance of 0.75 ± 0.08 mW/mm^2 in 2- to 4-week-old mice (Figure 1B). Photostimulation evoked more action potentials in older animals (Figure 1B), due at least in part to increased ChR2 expression (Figure S2B). Brief (5 ms), low-frequency flashes reliably evoked action potentials in MLIs from mice of all ages (Figure S2C). At higher frequencies of photostimulation, the roll-off frequency was 45 Hz in 2- to 4-week-old mice, whereas MLIs from 12-week-old mice responded to even higher-frequency flashes (Figure S2D).

ChR2-mediated circuit mapping requires focal photostimulation of presynaptic neurons. For this purpose, small (approximately 1 μm diameter in the focal plane) spots of laser light (405 nm, 4 ms) were scanned throughout the slice. The dye-filled MLIs in Figure 1C can be identified as a basket cell because its axons have terminal basket structures (arrows). When the laser spot was positioned over its cell body, an action potential was elicited (position 2, Figure 1D), whereas light-induced depolarizations were smaller at other locations (such as positions 1 or 3). By correlating the amplitude of responses with the location of the light spot that elicited them, we could map the light sensitivity of the MLIs (Wang et al., 2007; Schoenenberger et al., 2008). In Figure 1D, locations that elicited an action potential are shown in red, whereas locations eliciting subthreshold (or no) responses are not color coded. Superimposing this map upon the structure of the basket cell (Figure 1E) makes clear that action potentials were evoked only when the light spot was near the soma.

We refer to the area over which light was capable of evoking action potentials as the "optical footprint." MLI optical footprint size depended upon laser power: higher power increased the optical footprint (Figure S3A), due to the brighter light spots activating more ChR2 (Schoenenberger et al., 2008). To optimize the spatial resolution, we used the lowest laser power (0.54 mW) that reliably elicited action potentials when the light spot was focused on the cell bodies of ChR2-expressing MLIs. Under these "minimal photostimulation" conditions, the median area of MLI optical footprints (n = 59) was 5.5 × 10^3 μm^2 (Figure 1F). This median area can be approximated by a circle with a radius of 42 μm, indicating that the spatial resolution of MLI photostimulation was approximately 42 μm under our conditions.

In the example shown in Figure 1E, light spots only evoked action potentials when positioned over the cell body or proximal dendrite of the basket cell. To determine whether this was a general feature of "minimally photostimulated" MLIs, we examined the spatial overlap between optical footprints and axons in a subset of 15 dye-filled MLIs whose axons could be clearly resolved

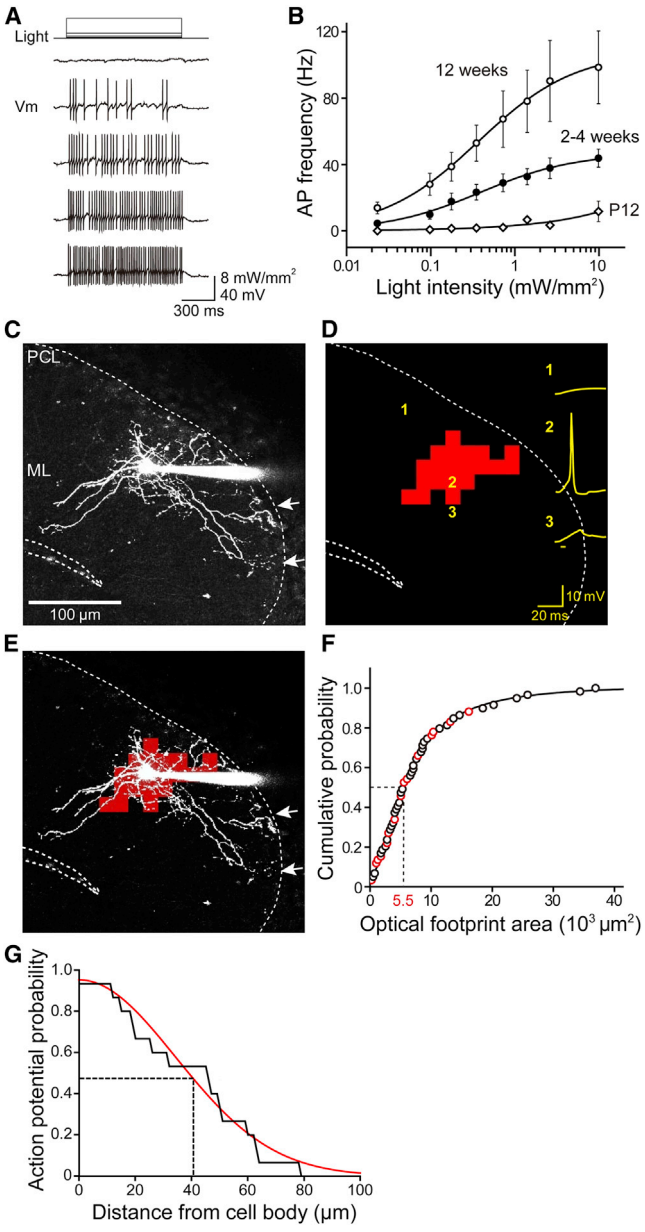

Figure 1. Photostimulation of MLIs

(A) Light-evoked changes in membrane potential (V_m) in ChR2-expressing MLIs. Action potential frequency increased with increasing light intensity.

(B) Relationship between light intensity and frequency of light-evoked action potentials (AP) in MLIs from transgenic mice of different ages. Curves are fits of the Hill equation. Data represent mean ± SEM. P12, n = 8; 2–4 weeks, n = 18; 12 weeks, n = 8.

(C) Structure of a basket cell in the molecular layer (ML) filled with Alexa 594 dye via a patch pipette (right). Arrows indicate basket structures formed by the neuron in the PC layer (PCL).

(D) Scanning a laser light spot across the brain slice, while simultaneously measuring membrane potential changes (yellow) in the ChR2-expressing basket cell, revealed locations where photostimulation evoked action potentials in the basket cell. Red indicates the locations where action potentials were induced, and the sum of these is the optical footprint of the basket cell. Numbers indicate positions where photoresponses shown at right were evoked, and bar below traces indicates light flash timing.

(E) Merger of basket cell image in (C) and optical footprint in (D) reveals that action potentials were evoked around the cell body and main dendritic region of the basket cell. Arrows indicate the terminal basket structures of basket cell axons.

(F) Cumulative probability distribution of MLI optical footprint areas. Areas of optical footprints were measured in either cell-attached recordings (black circles) or whole-cell recordings (red circles). Median optical footprint area (dashed lines) was 5.5 × 10^3 µm² (n = 59).

(G) Probability of overlap between axon and optical footprint (area where the light spots evoked action potentials in MLIs) over the distance of axon from cell body (n = 15). The light spots evoked action potentials only over axonal regions that are near the cell body. Data are fit with a Gaussian function (red curve), and half-width at half-maximum probability was 41 µm (dashed line).

over a substantial length (Figures S3B and S3C). On average, light spots evoked action potentials along only 28.2% ± 5.5% of the pixels overlying axons, and these pixels were all adjacent to MLI somata. The half-width of the distribution of sensitive axonal pixels was 41 µm away from the cell body (Figure 1G), which closely corresponds to the 42 µm spatial resolution of photostimulation. Thus, it appears that action potentials generated when light spots are focused on axonal regions near the cell body arise from somatic photostimulation, presumably because the somatic region has a larger surface area and, thus, more ChR2 available for activation within the light beam. Because illumination of MLI axons does not generate action potentials during "minimal photostimulation," we could use light-induced postsynaptic responses to locate MLI cell bodies/proximal dendrites in the circuit-mapping experiments described next.

Mapping the Spatial Organization of Local Inhibitory Circuits

Photostimulation of MLIs over a broad area (~0.23 mm²) of the slice inhibited action potential firing in PCs (Figure 2A), due to light-induced inhibitory postsynaptic currents (IPSCs) in the PCs (Figure S2E). Inhibition of PC firing increased with light intensity, with half-maximal inhibition observed at 0.15 ± 0.01 mW/mm² (Figures 2B and S2F). This increase in inhibition presumably was caused by more MLIs firing at higher light levels (Figure 1B). Inhibitory responses were blocked by the $GABA_A$ receptor antagonist, bicuculline (n = 9; Figure S2E), as expected for the inhibitory synapse between MLIs and PCs. Responses to light were never observed in bicuculline-treated PCs, confirming the absence of ChR2 expression in PCs.

To map the spatial organization of local inhibitory circuits between MLIs and PCs, we scanned the "minimal photostimulation" laser light spot (0.54 mW) in sagittal slices while correlating light spot location with the amplitude of resulting IPSCs in PCs (Wang et al., 2007; Petreanu et al., 2007). In the example shown in Figure 2C, light-evoked IPSCs were observed in discrete regions over a width of approximately 300 µm within the molecular layer (Figure 2C1). Comparison of this map to the structure of the postsynaptic PC (Figure 2C2) indicates that some IPSCs were elicited at locations within the PC dendritic field, whereas others were evoked well beyond the PC (Figure 2C3).

Occasionally, responses could be observed when the light spot was not in the molecular layer. In some of these cases, MLIs apparently were photostimulated when the light spot was

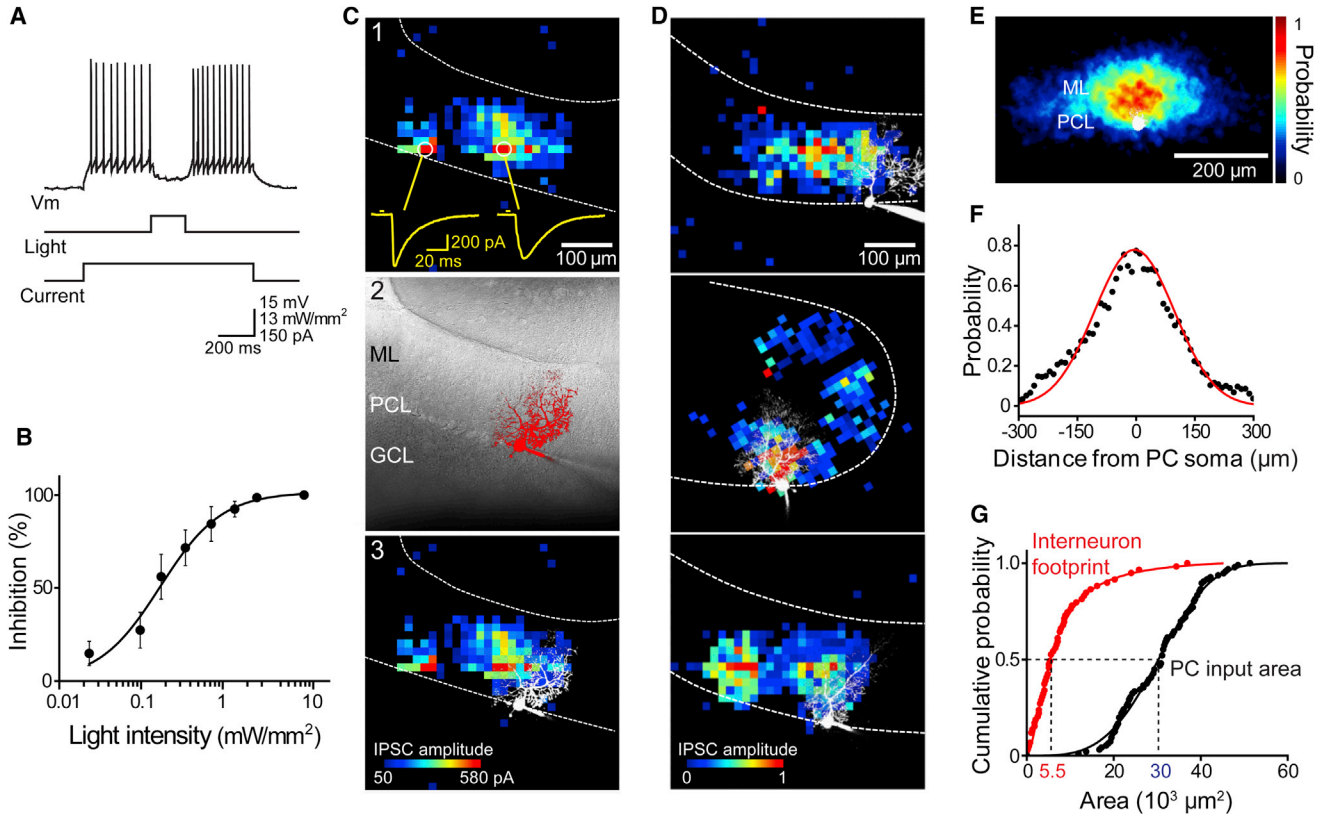

Figure 2. Photostimulation Mapping of Local Inhibitory Circuits

(A) Optogenetic control of MLI-PC synapses. Photostimulation of MLIs (middle trace) inhibited firing of a PC (top trace), which was depolarized by current injection (bottom trace).

(B) Relationship between light intensity and degree of inhibition of PC firing (n = 8). Data represent mean ± SEM.

(C) Photostimulation mapping of presynaptic ChR2-expressing MLIs. "1," locations are shown where a laser light spot evoked IPSCs in a PC. Examples of light-evoked IPSCs are shown as yellow traces below. Bar above traces indicates time of light flash. "2," an image of a PC filled with Alexa 549 dye is shown. ML, molecular layer; PCL, PC layer; GCL, granule cell layer. "3," merger of map in (C1) and image in (C2) shows the spatial relationship between the postsynaptic PC and its presynaptic inputs. IPSC amplitude is indicated by the pseudocolor scale shown below.

(D) Three examples of PC inhibitory input maps. IPSC amplitude was normalized relative to the largest response measured in each cell and is indicated by the scale shown below. Images of dye-filled PCs are superimposed in white.

(E) Spatial distribution of inhibitory inputs was obtained by aligning many input maps (n = 39) and averaging the probability of evoking IPSCs at a given location (scale at right) across the maps. PC somata are shown in white, and sagittal plane of the molecular layer runs from left to right.

(F) A line scan (black points) along the sagittal axis of the map shown above reveals the spatial distribution of input probability within the molecular layer. Red curve is a Gaussian fit.

(G) Calculation of MLI convergence onto PCs. Comparison between the cumulative probability plots of input field areas of PCs (black, n = 96) and MLI optical footprints (red, n = 59) indicates that the median value (dashed lines) of the input areas is 5.5 times larger than the median of the optical footprints. This means that at least five to six interneurons provide inhibitory inputs to a PC.

at the boundary between the granule cell layer and the PC layer (e.g., Figures 3B and 4A). These cases presumably arise from the 42 µm spatial resolution for photostimulation: a light spot positioned as much as 42 µm into the granule cell layer could still photostimulate MLIs at the bottom of the molecular layer. In addition, apparent single-pixel responses could be observed occasionally (e.g., stray blue pixels at the top of Figure 2C1). Given the size of the MLI optical footprint, these single-pixel responses are too small to result from photostimulation of MLIs and instead presumably reflect IPSCs caused by spontaneous action potential firing in MLIs (Häusser and Clark, 1997). Such IPSCs were excluded from our analysis of circuit convergence.

MLI-PC input maps exhibited many common features across experiments (Figures 2C and 2D). In all cases, the maps were somewhat noisy, with IPSC amplitude fluctuating substantially from pixel to pixel, even for adjacent pixels. This presumably is due to variable transmission at the MLI-PC synapse (Vincent and Marty, 1996; Pouzat and Hestrin, 1997): peak IPSC amplitude fluctuated widely even when the light spot was maintained in a fixed position (Figure S4). Mean IPSC amplitudes also varied for individual experiments, ranging from approximately 0.1–1 nA, with an overall mean of 156 ± 25 pA (n = 20). This value is consistent with the size of unitary synaptic responses observed over the age range we considered

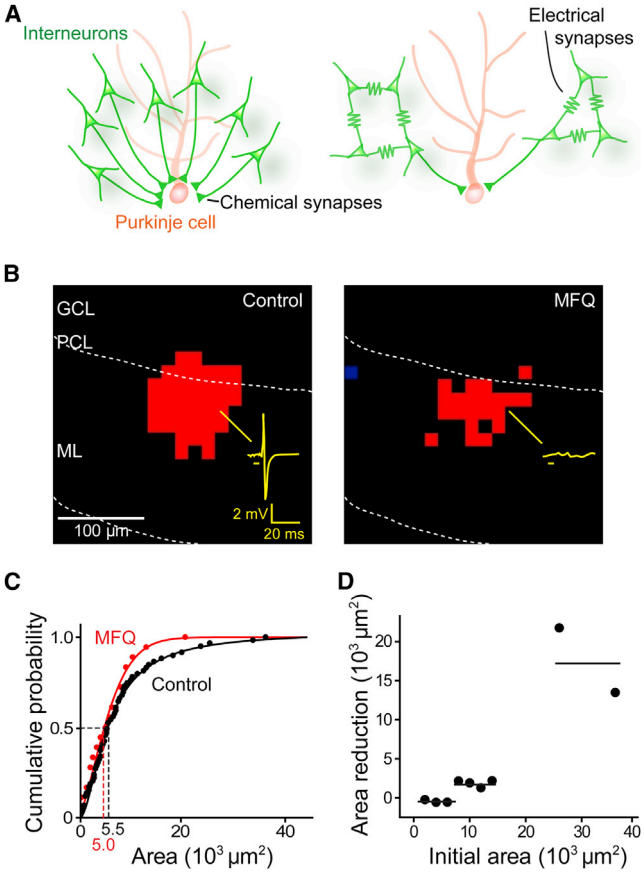

Figure 3. Cerebellar Interneurons Are Electrically Coupled

(A) Two models for the convergence of MLI inputs onto a PC, distinguished according to the absence (left) or presence (right) of contributions from electrical synapses between MLIs.

(B) Optical footprints of interneurons were reduced by blocking electrical synapses with MFQ (50 μM). Interneuron responses to light were recorded in the cell-attached configuration, with an example of a light-evoked action potential illustrated by the yellow trace in the left panel. Bar below trace indicates light flash timing, and red pixels indicate locations where light evoked action potentials in the absence (left) and presence (right) of MFQ. ML, molecular layer; PCL, PC layer; GCL, granule cell layer.

(C) Comparison of optical footprint area of MLIs in control conditions (black) and in the presence of MFQ (red).

(D) Relationship between optical footprint area and the reduction of footprint area caused by MFQ treatment. MLIs with the largest optical footprints showed the largest reductions in optical footprint area in response to MFQ treatment. Points indicate footprint areas, binned in 2,000 μm^2 intervals, whereas horizontal lines indicate hypothetical trends in the relationship.

(P21–P34; Pouzat and Hestrin, 1997). Thus, it appears that at any single location, the light spot activated a small number of presynaptic MLIs, perhaps only one, and this evoked IPSCs of fluctuating amplitudes. In Figure 2D and subsequent maps, IPSC amplitudes were normalized to the largest IPSC measured in each experiment to facilitate comparison across experiments.

IPSCs were evoked over a broad region within the molecular layer. Most of the input area extended beyond the PC dendrite, in one direction along the sagittal axis, and is probably due to activation of presynaptic basket cells. Input areas within the dendritic arbor of PCs may represent activation of presynaptic stellate cells. To visualize the overall spatial structure of the population, we aligned many input maps (n = 39) by using the PC soma as a fiducial mark and the location of the PC layer to align the x axis of each 2D map. We then determined the probability of observing an IPSC in each pixel within each individual map and averaged these to yield the mean probability map shown in Figure 2E. When measured along the molecular layer, parallel to the PC layer, this probability map extended over approximately 600 μm and was roughly Gaussian in shape, with a half-width of 250 μm (Figure 2F).

Many of the input field maps consisted of multiple discrete areas (Figures 2C and 2D), suggesting that they arose from multiple, dispersed MLIs. To estimate the number of MLIs converging upon a PC, we calculated the area of the inhibitory input field (Figure 2G, black) and compared this to the optical footprint (Figure 1F) of single photostimulated MLIs (Figure 2G, red). The median area of inhibitory inputs to a PC was 3.0 × 10^4 μm^2 (n = 96), which is 5.5 times larger than the median optical footprint of MLIs (5.5 × 10^3 μm^2; n = 59). This ratio indicates that a minimum of five to six interneurons provide converging inhibitory inputs to a single PC. After correcting for the 12% of MLIs that do not express ChR2, this estimate of MLI convergence rises to seven (see Discussion).

Clustered Electrical Coupling of Cerebellar Interneurons

The simplest interpretation of our finding that seven MLIs converge upon a PC is that each MLI forms chemical inhibitory synapses with the PC (Figure 3A, left). However, it is known that strong electrical synapses occur between MLIs (Mann-Metzer and Yarom, 1999; Alcami and Marty, 2013), and these could electrically couple MLIs and thereby amplify the effects of a smaller number of direct, chemical inputs (Figure 3A, right). To distinguish between these two models, we examined the effects of disrupting electrical synapses: the model shown in Figure 3A (right) predicts that such disruption should reduce the number of converging interneurons and thereby reduce the input area, whereas the model of Figure 3A (left) predicts little or no effect.

To inhibit electrical synaptic transmission, we treated slices with three different gap junction blockers: meclofenamic acid (MFA) and carbenoxolone (CBX), as general blockers of gap junctions (Pan et al., 2007), as well as mefloquine (MFQ), which has been reported to be a more selective blocker of gap junctions containing connexin 36 (Cruikshank et al., 2004). Connexin 36 is thought to be the predominant component of gap junctions in CNS neurons (Connors and Long, 2004), is found in the molecular layer (Helbig et al., 2010), and is thought to mediate electrical coupling between MLIs (Alcami and Marty, 2013).

We examined the ability of these compounds to inhibit electrical synaptic transmission between MLIs by examining their effects on high-frequency "spikelets," which result from electrical transmission of action potentials between neighboring MLIs (Mann-Metzer and Yarom, 1999; Alcami and Marty, 2013). Wide-field photostimulation of MLIs, in the presence of chemical synapse blockers, produced both photocurrents due to

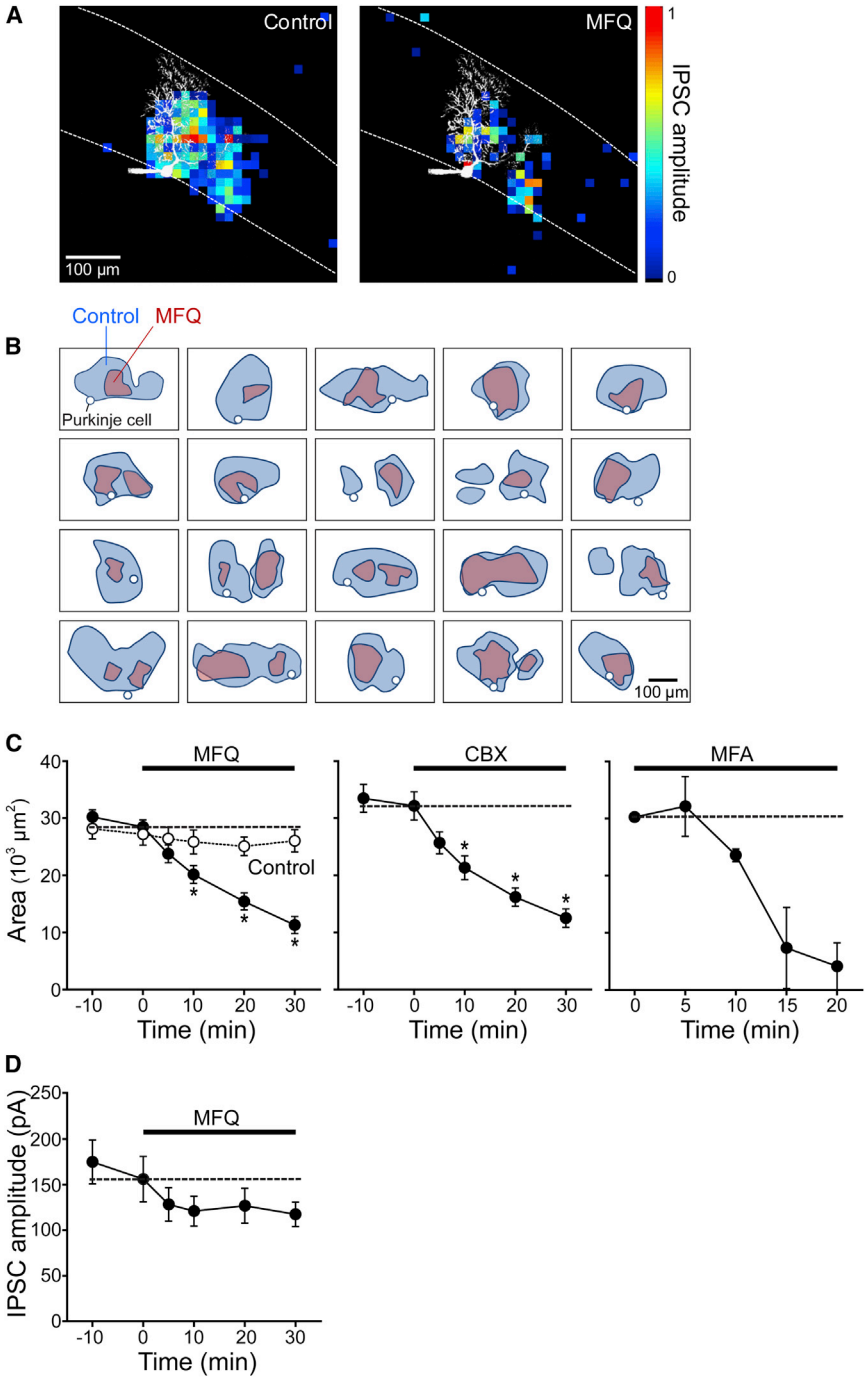

Figure 4. Electrical Synapses Contribute to Inhibitory Input Field of PCs

(A) The area of the inhibitory input field of a PC (left panel) was reduced by treatment with MFQ (50 μM; right panel). Pseudocolor scale indicates the normalized amplitude of light-evoked IPSCs for each location. Image of dye-filled PC is shown in white.

(B) Gallery of input field maps measured for 20 different PCs before and after MFQ treatment. Outlines of input fields measured in control conditions are shown in blue, and those measured in the same experiments after MFQ treatment are shown in pink. In every case, MFQ treatment reduced the area of the input field. White circles indicate the location of somata of PCs used for input field determinations.

(C) Time course of changes in the mean area of inhibitory input field of IPSCs during MFQ (50 μM, n = 20), CBX (200 μM, n = 18), and MFA (200 μM, n = 2) treatment. Asterisks indicate time points where drug treatment caused significant ($p < 0.001$) reductions. Data represent mean ± SEM.

(D) Time course of changes in the mean amplitude of IPSCs during MFQ treatment. Although input field area was significantly reduced by MFQ (C), IPSC amplitude was not (D). Data represent mean ± SEM.

activation of ChR2 expressed in the neuron as well as spikelets caused by light-evoked action potentials in other MLIs (Figure S5A, arrow). These spikelets were eliminated by each gap junction blocker, indicating that these drugs block electrical synaptic transmission between the MLIs (Figures S5A–S5C, bottom). Because MFA also significantly reduced the excitability of MLIs, we largely avoided its use. CBX reduced the amplitude of evoked IPSCs (Figure S6C; Tovar et al., 2009) and increased PC holding current but did not affect the excitability of MLIs. On the other hand, MFQ had little effect on the electrical characteristics of MLIs (Figures S5D–S5G). Its only noticeable side effect was an increase in the amplitude and frequency of excitatory miniature postsynaptic currents (Figures S5H and S5I), which was not produced by CBX or MFA (Figures S5J and S5K; Cruikshank et al., 2004). To evaluate the contribution of electrical coupling to MLI convergence, we relied mainly on MFQ.

Treatment of slices with MFQ (50 μM) reduced the area over which photostimuli evoked action potentials in MLIs (Figure 3B). MFQ reduced the median optical footprint of MLIs from 5.5 × 10^3 μm^2 (n = 59) to 5.0 × 10^3 μm^2 (n = 18; Figure 3C), indicating that transmission through electrical synapses contributes to the optical footprint of MLIs. MFQ selectively reduced larger optical footprints (those with areas >6,000 μm^2) while sparing smaller ones (Figure 3C). This was most evident in a subset of experiments where the optical footprints of the same MLIs were analyzed before and after MFQ treatment. In these experiments, there was a clear relationship between the size of the optical footprint prior to drug treatment and the reduction caused by MFQ: MLIs with relatively small optical footprints were largely unaffected by MFQ, whereas those with larger optical footprints were reduced (Figure 3D). Our interpretation is that the larger optical footprints

came from clusters of adjacent MLIs connected by electrical synapses, whereas smaller footprints arose from MLIs that were not well coupled to other MLIs. Thus, transmission of spikes through electrical synapses creates local networks of clustered MLIs.

Blocking Electrical Synapses Reduces Interneuron Convergence

We next asked whether gap junction blockers affect the organization of inhibitory circuits between MLIs and PCs. MFQ dramatically decreased the area of the inhibitory input field of the PC shown in Figure 4A. This was a general observation: Figure 4B shows results from 20 experiments where input fields were compared before (blue) and during (pink) MFQ treatment. In every case, the input area was reduced substantially by MFQ. The area of input fields gradually declined after MFQ treatment (Figure 4C, left), with this area decreasing by 60% after 30 min ($p < 0.001$ compared to pretreatment, ANOVA with Tukey's test; $n = 20$) and then remaining constant. In control conditions, where the slices were exposed to the DMSO (0.05%) used as a drug solvent, input field area was constant over the measurement period (Figure 4C, left). CBX similarly reduced input field area (Figure 4C, center, and Figures S6A and S6B), as did MFA (Figure 4C, right), indicating that this reduction is due to blockade of electrical synapses. Together, these results provide strong evidence that electrical coupling increases the convergence of MLIs onto PCs, as in the model of Figure 3A (right).

This model also predicts that the loss of gap junctions should not affect the amplitude of light-evoked IPSCs, which will be determined only by the strength of the synapses of the MLIs that directly innervate PCs. Indeed, although MFQ decreased input area substantially, the mean amplitude of IPSCs evoked within the input area was not affected by MFQ treatment (Figure 4D; no significant difference between any group, $p = 0.19$, ANOVA). This result thus provides a second line of support for the model.

The model makes two other predictions regarding the kinetics of the light-evoked IPSCs. It predicts that the latency of the fastest IPSCs should reflect the kinetics of synaptic transmission at the synapses of MLIs that directly innervate the PC, whereas longer latencies should be associated with disynaptic IPSCs produced by photostimulating MLIs that do not directly innervate PCs. Thus, the model predicts that blocking gap junctions should have little effect on the minimal latency of IPSCs yet should speed up IPSC time to peak. Both of these predictions were borne out in experimental measurements: MFQ had little effect on the latency of IPSCs (Figures 5A and 5B), while markedly accelerating IPSC time to peak (Figures 5C and 5D). MFQ treatment caused a small but statistically significant ($p < 0.01$, paired t test) decrease in the mean value of IPSC initial latency, with this latency changing from 10.4 ± 0.2 ms in control conditions to 9.9 ± 0.2 ms in the presence of MFQ ($n = 20$). This decrease in latency is due to a slight decrease in the latency of action potential generation in the presynaptic MLIs, from 9.6 ± 0.6 ms in control conditions to 8.8 ± 0.6 ms in the presence of MFQ ($n = 18$), as expected when MLIs are uncoupled. In contrast, MFQ treatment greatly accelerated IPSC mean time to peak from 5.6 ± 0.5 ms to 3.3 ± 0.2 ms ($n = 20$; $p < 0.001$, paired t test). As predicted, IPSCs with long times to peak were selectively affected, indicating that these are likely to result from a disynaptic (MLI-MLI-PC) circuit (Figure 5D). This was particularly evident in spatial maps of IPSC times to peak: in the example shown in Figure 5C, MFQ caused a selective loss of the cluster of pixels with long times to peak while sparing the adjacent cluster with short times to peak. Our interpretation is that the cluster of pixels with short times to peak represents photostimulation of MLIs that directly innervate the PC, whereas those with long times to peak reveal the location of MLIs that are indirectly coupled via electrical synapses. Consistent with this interpretation, IPSCs with long times to peak sometimes had inflections on their rising phase, suggesting delayed disynaptic inputs, whereas those with rapid times to peak usually did not (Figure 5E). MFQ treatment preferentially reduced the number of inflections on slow-rising IPSCs, yielding IPSCs with fast rise times (Figures 5E and 5F). The reduction in the number of IPSC inflections after MFQ treatment (Figure 5G) indicates that IPSCs with slow times to peak and multiple infections were mainly associated with MLIs connected disynaptically via electrical synapses. In summary, we conclude that electrical coupling increases the convergence of MLIs onto PCs (Figure 3A, right).

Quantifying the Contributions of Electrical and Chemical Synapses to MLI Convergence

The changes in input field area caused by blockade of electrical synapses provided two ways to quantify the contribution of electrical coupling to convergence of MLIs onto PCs. First, we examined the structure of the input fields after treatment with gap junction blockers. In many experiments (14 out of 38), including the example shown in Figure 4A, MFQ (and CBX) caused the input field to fragment into 2 smaller areas, indicating the presence of at least 2 different presynaptic MLIs. The mean area of the fragmented input fields was $6.2 \pm 0.7 \times 10^3$ μm^2, which is not different ($p = 0.96$, t test) from the mean area of MLI optical footprints measured after blockade of gap junctions, which was $6.3 \pm 1.2 \times 10^3$ μm^2. The similarity of these two values indicates that these cases reflect input from just two presynaptic MLIs whose optical footprints do not overlap.

Next, we used our entire data set to calculate the number of MLIs converging on a PC in the presence of gap junction blockers. The median area of input fields measured after blocking gap junctions was 8.8×10^3 μm^2 ($n = 38$), whereas the median optical footprint of single MLIs under similar conditions was 5.0×10^3 μm^2 ($n = 18$). The ratio of these two values is 1.8 (Figure 6A), indicating that on average, approximately two MLIs directly converge upon a PC. This is in good agreement with our observation that gap junction blockers often fragmented input fields into two parts. Thus, on average, approximately two MLIs form functional inhibitory synapses with a PC. As described above, seven MLIs converge onto a PC in control conditions (Figure 2G), meaning that on average, five MLIs converge indirectly via electrical synapses, as depicted in Figure 3A (right).

To determine the spatial organization of inputs after electrical synapses were blocked, we calculated the input probability map in MFQ-treated slices (Figure 6B, upper; $n = 20$). Although MFQ significantly reduced the overall probability of coupling, there was relatively little change in the width of this distribution (Figure 6B, lower). Gaussian fits to these data had full-widths

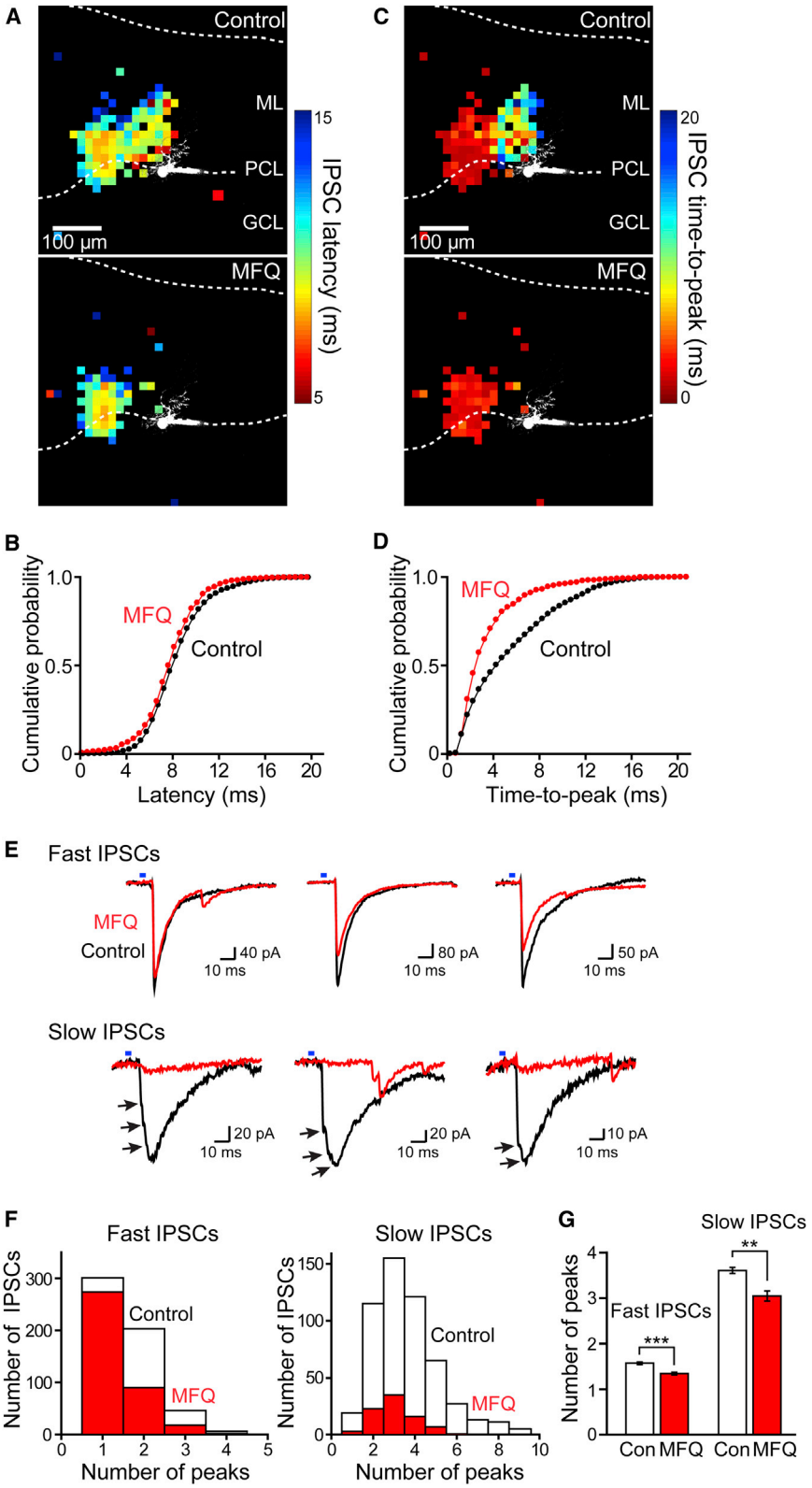

Figure 5. Effect of Gap Junction Blockers on IPSC Kinetics

(A) Map of latency of IPSCs evoked by photostimulation at different locations before (upper panel) and after (lower panel) MFQ treatment. Pseudocolor scale (right) indicates the latency of these IPSCs, with shorter latencies indicated by hotter colors. Image of dye-filled PC is shown in white. ML, molecular layer; PCL, PC layer; GCL, granule cell layer.

(B) Cumulative distribution of IPSC latencies measured for all locations (n = 20 experiments) in control conditions (black) and in the presence of MFQ (red).

(C) Map of time to peak of IPSCs evoked by photostimulation at different locations measured before (upper panel) and after (lower panel) MFQ treatment. Pseudocolor scale (right) indicates IPSC time to peak, with faster times to peak indicated by hotter colors. Image of dye-filled PC is shown in white.

(D) Cumulative distribution of IPSC times to peak measured for all locations (n = 20 experiments) in control conditions (black) and in the presence of MFQ (red). IPSC time to peak became significantly faster after MFQ treatment, with selective loss of slower responses.

(E) Examples of fast (time to peak <4 ms) and slow (time to peak >4 ms) IPSCs from the maps of (A) and (C). Black traces were recorded in control conditions, whereas the red traces were recorded in response to photostimulation of the same location after MFQ treatment. Slow IPSCs typically had multiple inflections on their rising phase, whereas fast IPSCs usually did not. Arrows indicate inflections/peaks on the slow IPSC traces. After treatment with MFQ, slow IPSCs were preferentially lost.

(F) Histogram of number of inflections/peaks in fast IPSCs (time to peak <4 ms) and slow IPSCs (time to peak >4 ms) before (white) and after (red) MFQ treatment in the subset of experiments (n = 10 experiments). Compared to fast IPSCs, slow IPSCs tended to have more inflections, and those with multiple inflections were more affected by MFQ treatment.

(G) Changes in the average of number of inflections/peaks in fast and slow IPSCs after MFQ treatment (n = 10 experiments). Con (white) indicates control measurements, whereas MFQ (red) is after MFQ treatment. MFQ significantly reduced the number of inflections in IPSCs. Data represent mean ± SEM.

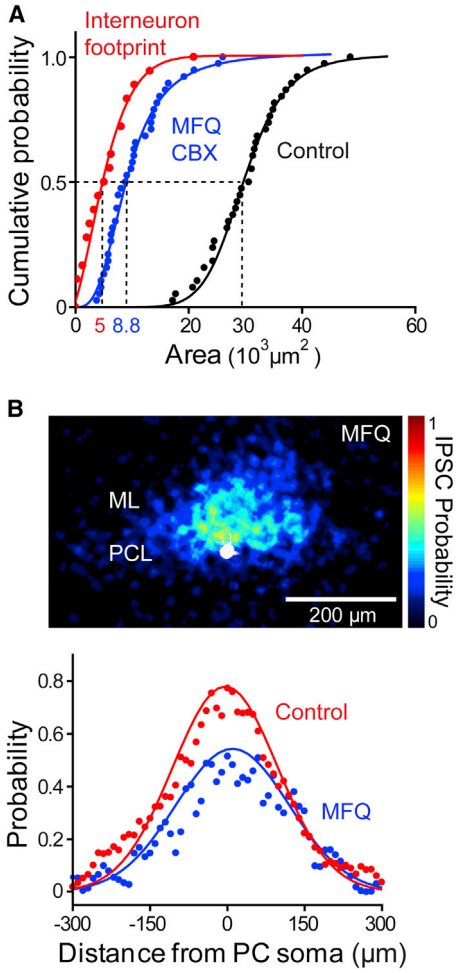

Figure 6. Quantification of the Contribution of Electrical Synapses to Interneuron Convergence

(A) Calculation of amount of convergence of interneuron inputs onto a PC, as in Figure 2G, in control conditions (black) or in the presence of a gap junction blocker (CBX or MFQ; blue, n = 38). Median area of input fields measured after blocking electrical synapses (8.8×10^3 μm^2) was almost 3-fold smaller than in control conditions (3.0×10^4 μm^2) but was 1.8-fold larger than the area of MLI optical footprints (5.0×10^3 μm^2, n = 18) measured in the presence of gap junction blockers (red). This indicates that MLI circuits providing inhibitory inputs to a PC consist of roughly two direct chemical synapses with several additional MLIs converging via electrical synapses.

(B) Upper: spatial distribution of inhibitory inputs (upper panel) measured in the presence of MFQ, determined as in Figure 2E (n = 20). PC somata are shown in white, and pseudocolor scale indicates the probability of evoking an IPSC at a given location. Lower view is a line scan (blue points) along the sagittal axis of the map shown above reveals that whereas the overall probability of evoking an IPSC was significantly reduced after MFQ treatment, there was little change in the overall spatial distribution of inhibitory inputs in comparison to control conditions (red points). Continuous curves indicate fits of Gaussian functions.

(half-maximum) of 250 μm in control conditions (Figure 6B, red) and 260 μm in the presence of MFQ (blue). This indicates that the local circuits of electrically coupled MLIs are distributed both laterally and medially relative to the MLIs that are directly connected to PCs by chemical synapses (see Figures S6D–S6F). Moreover, the observation that the amplitude of IPSCs was not significantly changed after blocking gap junctions (Figure 4D) suggests that the two MLIs directly innervating a PC are not electrically coupled to each other; if they were coupled, then both would fire action potentials, leading to larger IPSCs. Therefore, inhibitory circuits in the cerebellar molecular layer consist of chemical and electrical synapses that create specific spatial patterns of convergence onto PCs.

Electrical Coupling Is Spatially Biased

The cerebellum is a highly polarized structure (Palay and Chan-Palay, 1974), with many cellular elements oriented in either the sagittal plane (e.g., PC dendrites) or the coronal plane (e.g., parallel fibers). Although MLI dendrites are planar and sagittally oriented, their axonal projections enter different planes (Palay and Chan-Palay, 1974) and can form axo-axonic electrical synapses with each other (Alcami and Marty, 2013). Thus, it is not clear whether inhibitory inputs from MLIs to PCs exhibit any spatial bias. We addressed this by examining local inhibitory circuits at different planes of section: the cerebellum was sliced at angles of 30°, 60°, or 90° relative to the sagittal plane. In the coronal plane (90°), MLI input fields were narrower and located closer to PCs in comparison to input fields in the sagittal plane (Figures 7A and 7D). Intermediate planes of section yielded input fields of intermediate properties, with the width of the averaged input map reduced with increasing angle (Figures 7B and 7C). This is expected if molecular layer inhibitory circuits are mainly organized in the sagittal plane: in coronal slices, connected MLIs will lie on top of each other and will be orthogonal to the surface of the slice. Consistent with this interpretation, in coronal slices, MLI optical footprints (Figure S7A) were similar in shape and size to the input fields measured in PCs (Figures 7A and 7D). In sum, our results indicate that inhibitory circuits in the molecular layer are sagittally organized, as are the dendrites of the postsynaptic PCs.

To examine the organization of electrical synapses between MLIs, the effects of MFQ were compared at each orientation. Remarkably, the effect of blocking electrical synapses depended upon the orientation of the plane of section: whereas MFQ produced a prominent reduction in the input area in sagittal slices, as described above, it had virtually no effect in coronal slices (Figures 7D and 7E). Slices from intermediate planes of section showed intermediate effects of MFQ. Quantification revealed that the degree of block by MFQ depends upon the plane of section, with no significant effect observed in coronal slices (Figure 7F). As was the case for sagittal slices, in coronal slices, MFQ hastened IPSC time to peak (Figures S7B and S7C). These results indicate that electrical transmission between MLIs is spatially biased: whereas electrical coupling is prominent in the sagittal plane, it is absent in the coronal plane. Our conclusions regarding the spatial organization of MLI synaptic circuitry are diagrammed in Figure 7G.

DISCUSSION

We used an optogenetic approach to map local inhibitory circuits in the cerebellar cortex. In addition to providing information about the functional organization of the inhibitory circuits between MLIs and PCs, our results also revealed the organization of electrical synapses between MLIs.

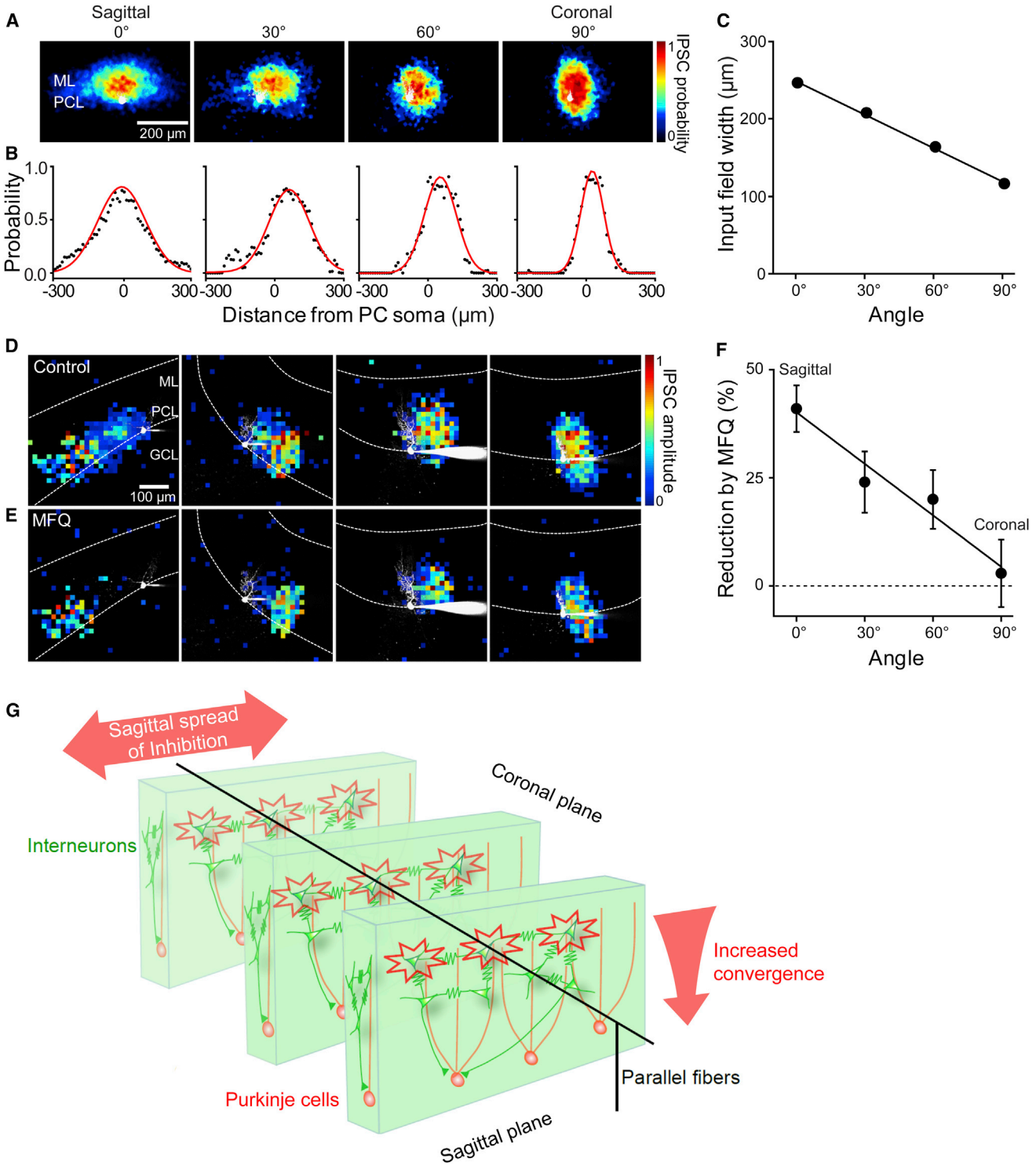

Figure 7. Electrical Coupling between Interneurons Is Spatially Biased

(A) Averaged probability maps of IPSC input fields measured in cerebellar slices cut at different angles; 0° and 90° indicate data from sagittal and coronal slices, respectively. PC somata are shown in white. ML, molecular layer; PCL, PC layer. Sample sizes are 0° (39), 30° (12), 60° (10), and 90° (14).

(B) Line scans (black) across the widths of the averaged probability maps shown in (A) reveal that the spatial distribution of presynaptic MLI inputs varies according to the angle of slicing. Data are fit to Gaussian functions (red curves).

(C) Relationship between slicing angle and widths of IPSC probability maps. Width was calculated as the full width at half-maximum for Gaussian fits to the line scans shown in (B) and decreased as the slicing angle was increased.

(legend continued on next page)

Our mapping was based on focal photostimulation of cerebellar MLIs expressing ChR2 (Wang et al., 2007; Petreanu et al., 2007). With this approach, we could establish the spatial organization of circuits with higher cellular specificity than possible with mapping via glutamate uncaging (Callaway and Katz, 1993) and with greater speed compared to paired electrophysiological recordings (Mann-Metzer and Yarom, 1999). Photostimulus intensity was carefully controlled ("minimal photostimulation") to restrict suprathreshold activation to regions near MLI cell bodies (Figure 1E) because spatial resolution is degraded appreciably by more intense photostimulation (Figure S3A; Schoenenberger et al., 2008) or by the use of larger light spots (Cruikshank et al., 2010). Future use of two-photon excitation could further improve spatial resolution, particularly in the z axis (Rickgauer and Tank, 2009).

Functional Organization of Local Inhibitory Circuits

The improvement in throughput associated with our technique allowed us to analyze many input field maps and thereby provide a quantitative description of the spatial organization of this circuit. By comparing the optical footprint for photostimulation of single MLIs with the size of the input field where photostimulation evoked IPSCs in postsynaptic PCs, we estimated that six MLIs converge onto a single PC. Because approximately 12% of MLIs do not express ChR2, this reflects a convergence ratio of approximately seven; thus, we conclude that at least seven MLIs converge on a PC. This is in line with previous anatomical estimates of six to ten basket cells innervating a PC (Palay and Chan-Palay, 1974; Vincent et al., 1992) and functional estimates of five to nine MLIs converging on a PC (Häusser and Clark, 1997; Park et al., 2012), though we consider our determination to be more precise because we obtained both structural and functional information together and also could take into account the contribution of electrical synapses between MLIs.

Our analysis provides quantitative information about the spatial organization of functional circuits. Individual maps usually revealed some inputs arising from within the dendritic arbor of the PC, with others observed laterally more than 300 μm away from the PC soma. Although a given input field was usually skewed toward one side of the PC dendrites (Figures 2C and 2D), on average, the distribution was symmetrical and spread approximately 300 μm in each direction (Figures 2E and 2F). This is comparable to the length of 250–350 μm reported for axonal arbors of MLIs (Gao et al., 2006). This information will allow construction of more realistic computational models of the role of local inhibitory circuits in information processing.

Spatial Coordination of Interneurons via Electrical Synapses

Gap junctions were first observed between MLIs by electron microscopy (Sotelo and Llinás, 1972), studies that were later extended by demonstration of electrical and dye coupling of MLIs (Mann-Metzer and Yarom, 1999). Simultaneous recordings from pairs of neighboring MLIs have revealed that 40% of all MLI pairs are electrically coupled (Mann-Metzer and Yarom, 1999; Alcami and Marty, 2013). The coupling coefficient between these neurons is variable but has a mean value of 0.12, which is somewhat higher than that reported for other interneuron networks (Galarreta and Hestrin, 2001). As expected for electrical synapses with a coupling coefficient greater than 0.1 (Long et al., 2004), when photostimulating multiple MLIs we observed spikelets (Figures S5A–S5C) that presumably arise from action potentials in coupled MLIs (Mann-Metzer and Yarom, 1999; Alcami and Marty, 2013). MLIs are spontaneously active, and their resting membrane potential therefore is close to action potential threshold; this allows the small depolarization associated with spikelets to reach threshold and generate action potentials, thereby causing synchronous firing of MLIs (Mann-Metzer and Yarom, 1999; Hormuzdi et al., 2004).

The substantial electrical coupling between MLIs also plays an important role in the spatial organization of MLI circuits because blockade of electrical synapses reduced the optical footprint of MLIs (Figure 3C) and the size of MLI input fields onto PCs (Figures 4, 6, and 7). This was not due to drug side effects because (1) three different blockers had similar effects (Figure 4C); (2) the effects of MFQ on MLI optical footprints were selective for cells with large footprints (Figures 3C and 3D); (3) the effect of MFQ on input field area was only observed in sagittal slices, but not in coronal slices (Figure 7F); (4) MFQ treatment did not alter MLI electrical properties (Figures S5D–S5G); and (5) similar effects are observed in connexin 36 knockout mice (Alcami and Marty, 2013).

The reduction in MLI optical footprints by gap junction blockers (Figure 3D) indicates that there are local clusters of MLIs connected by electrical synapses. Because the effects of the blockers depend upon optical footprint size, these clusters apparently are heterogeneous, with some MLIs being connected to multiple partners, whereas others are solitary. Thus, electrical transmission extends the spatial range of activation of MLIs and has similar effects in neighboring Golgi cells (Vervaeke et al., 2012).

Disruption of MLI clusters reduced the area of the presynaptic input field of PCs (Figures 4A and 4B), indicating that electrical coupling between MLIs broadens the spatial convergence of local inhibitory synaptic inputs. Our quantitative analysis suggested that an average of two spatial domains, each consisting of clusters of three to four electrically coupled MLIs, provide individual chemical inputs to a PC (Figure 3A, right). These conclusions are consistent with recent electrophysiological results suggesting that each MLI is electrically coupled to one to four other MLIs (Alcami and Marty, 2013). Thus, spatial coordination

(D) Representative maps of IPSC input fields measured in slices cut at different angles. In all cases, images of dye-filled PCs are shown in white.
(E) Effect of MFQ treatment on maps of input fields measured for the same experiments shown in (D).
(F) Relationship between slicing angle and the reduction of input field area produced by MFQ treatment. Sample sizes are 0° (20), 30° (12), 60° (10), and 90° (14). The extent to which the area of the inhibitory input field was reduced by MFQ treatment decreased with increasing slicing angle, with MFQ having no effect in coronal slices. Data represent mean ± SEM.
(G) Diagram of the deduced spatial organization of circuits between MLIs (green) and PCs (pink). Electrical synapses between MLIs are biased and spatially coordinate interneurons only in the sagittal plane.

of MLIs via electrical synapses increases spatial convergence by amplifying the effect of the limited number of MLIs providing direct inhibitory drive to PCs. This extends to the brain observations that retinal electrical synapses enhance convergence of presynaptic neurons onto their postsynaptic targets (Bloomfield and Völgyi, 2009). Because transmission at electrical synapses can be modulated by neurotransmitters and other signals (Hatton, 1998; McCracken and Roberts, 2006), it is possible that the spatial coordination of MLIs via electrical synapses is dynamically controlled to fine-tune the amount and location of convergence.

Spatially Biased Electrical Coupling between Interneurons

Slices cut in different orientations allowed us to reconstruct the 3D organization of electrical connections between MLIs. Although blocking electrical synapses had a large effect on input field area in sagittal slices, no such effect was observed in coronal slices (Figures 7E and 7F). This indicates that electrical synapses between MLIs are spatially biased and oriented in the sagittal plane (Figure 7G). This remarkable feature has escaped detection by anatomical observations, though it is consistent with the experiment in Figure 5A of Mann-Metzer and Yarom (1999), suggesting that tracer-coupled MLIs are found mainly in the sagittal plane. After our paper was accepted, a paper by Rieubland et al. (2014) appeared and also concludes that electrical synapses between MLIs are biased in the sagittal plane and serve to create clusters of coupled MLIs.

The spatial bias of electrically coupled MLI networks may be important for local information processing in the cerebellar cortex. It appears that electrical synapses, in conjunction with the trajectory of MLI axons, determine the spatial range of lateral inhibition, which is thought to play an important role in shaping the temporal and spatial pattern of PC activation (Cohen and Yarom, 2000; Dunbar et al., 2004; Mittmann et al., 2005). The presence of electrically coupled clusters of MLIs in the sagittal plane will allow stronger inhibition to occur across the entire width of the PC dendritic tree (Figure 7G), thereby ensuring a precise pattern of synaptic inhibition in response to distinct patterns of parallel fiber input. Furthermore, the absence of electrical coupling in the coronal plane allows for discontinuous inhibition of PCs along a parallel fiber beam (Bower, 2010), as has been observed in response to sensory stimuli (Gao et al., 2006).

In conclusion, although it is well established that electrical synapses play an important role in temporally synchronizing neuronal activity (Mann-Metzer and Yarom, 1999; Beierlein et al., 2000), proposals that groups of electrically coupled neurons can create spatial compartments have received relatively little attention (Sotelo and Llinás, 1972; Galarreta and Hestrin, 2001; Rela and Szczupak, 2004). Three of our results make clear that electrical synapses play an important role in spatial coordination of interneurons in the cerebellar cortex: (1) clustering of adjacent MLIs via electrical synapses; (2) a remarkable bias in the spatial organization of electrical synapses in MLI networks; and (3) the influence of these networks on convergence of synaptic inhibition. Given the widespread occurrence of electrical synapses between interneurons throughout the brain, spatial coordination of interneurons may be a very general function for electrical synapses.

EXPERIMENTAL PROCEDURES

For further details, see the Supplemental Experimental Procedures.

Animals

BAC transgenic mice expressing ChR2 under the control of the nNOS promoter were generated. All procedures were conducted according to the Institutional Animal Care and Use Committee guidelines of the Biopolis Biological Resource Center, Duke University, Korea Institute of Science and Technology, and the Marine Biological Laboratory.

Anatomy and Immunohistochemistry

Mice (P21, P31, and P150) were perfused transcardially with 4% paraformaldehyde, and brains were cryosectioned into sagittal slices followed by staining with monoclonal mouse anti-GAD67 (1:1,000; Chemicon) and Alexa 555-conjugated goat anti-mouse antibody (1:200; Invitrogen). Sections were imaged with an epi-fluorescence microscope (Nikon Eclipse Ti) or a confocal microscope (Zeiss LSM510 META).

Brain Slice Recording

Cerebellar sections were prepared as previously described (Lee et al., 2010), and whole-cell patch-clamp recordings were made at room temperature. Electrical responses were acquired via a Multiclamp 700B amplifier (Molecular Devices) with Digidata 1440A interface (Molecular Devices).

Photostimulation and Analysis

Photostimulation was accomplished as previously described by Wang et al. (2007). In brief, for wide-field excitation, slices were exposed to blue light (465–495 nm) from a mercury arc lamp. For high-speed circuit mapping, photostimulation was done with a laser-scanning microscope (FV1000MPE; Olympus) equipped with ×25 NA 1.05 (Olympus XLPlan N) water-immersion objectives lens. A 510 × 510 μm area of the slice was scanned with a 405 nm laser spot (4 ms duration) in a 32 × 32 array of pixels, yielding a scanning interval of 16 μm. The laser spot was scanned in a pseudorandom sequence, to avoid photostimulation of adjacent pixels, while cellular responses were simultaneously measured in cell-attached or whole-cell patch-clamp recordings. Mapping data were analyzed with custom software to produce the synaptic input maps and averaged probability maps. Data are expressed as mean ± SEM.

SUPPLEMENTAL INFORMATION

Supplemental Information includes Supplemental Experimental Procedures, seven figures, and one table and can be found with this article online at http://dx.doi.org/10.1016/j.celrep.2014.04.047.

ACKNOWLEDGMENTS

We thank N. Chow for histological work, P. Namburi for software development, and H. Gill, M. Kee, and P. Teo for technical assistance. We also thank P. Alcami, P. Chadderton, E. DeSchutter, I. Llano, J. Mancuso, A. Marty, J. Medina, and J. Simpson for very helpful comments on this paper. This work was supported by a CRP grant from the National Research Foundation of Singapore and by the World Class Institute (WCI) Program of the National Research Foundation of Korea (NRF) funded by the Ministry of Education, Science and Technology of Korea (NRF grant number WCI 2009-003).

Received: August 7, 2012
Revised: February 10, 2014
Accepted: April 21, 2014
Published: May 22, 2014

REFERENCES

Alcami, P., and Marty, A. (2013). Estimating functional connectivity in an electrically coupled interneuron network. Proc. Natl. Acad. Sci. USA *110*, E4798–E4807.

Beierlein, M., Gibson, J.R., and Connors, B.W. (2000). A network of electrically coupled interneurons drives synchronized inhibition in neocortex. Nat. Neurosci. *3*, 904–910.

Bloomfield, S.A., and Völgyi, B. (2009). The diverse functional roles and regulation of neuronal gap junctions in the retina. Nat. Rev. Neurosci. *10*, 495–506.

Bower, J.M. (2010). Model-founded explorations of the roles of molecular layer inhibition in regulating purkinje cell responses in cerebellar cortex: more trouble for the beam hypothesis. Front. Cell. Neurosci. *4*, 1–16.

Callaway, E.M., and Katz, L.C. (1993). Photostimulation using caged glutamate reveals functional circuitry in living brain slices. Proc. Natl. Acad. Sci. USA *90*, 7661–7665.

Cohen, D., and Yarom, Y. (2000). Cerebellar on-beam and lateral inhibition: two functionally distinct circuits. J. Neurophysiol. *83*, 1932–1940.

Connors, B.W., and Long, M.A. (2004). Electrical synapses in the mammalian brain. Annu. Rev. Neurosci. *27*, 393–418.

Cruikshank, S.J., Hopperstad, M., Younger, M., Connors, B.W., Spray, D.C., and Srinivas, M. (2004). Potent block of Cx36 and Cx50 gap junction channels by mefloquine. Proc. Natl. Acad. Sci. USA *101*, 12364–12369.

Cruikshank, S.J., Urabe, H., Nurmikko, A.V., and Connors, B.W. (2010). Pathway-specific feedforward circuits between thalamus and neocortex revealed by selective optical stimulation of axons. Neuron *65*, 230–245.

Dizon, M.J., and Khodakhah, K. (2011). The role of interneurons in shaping Purkinje cell responses in the cerebellar cortex. J. Neurosci. *31*, 10463–10473.

Dunbar, R.L., Chen, G., Gao, W., Reinert, K.C., Feddersen, R., and Ebner, T.J. (2004). Imaging parallel fiber and climbing fiber responses and their short-term interactions in the mouse cerebellar cortex in vivo. Neuroscience *126*, 213–227.

Eccles, J.C., Ito, M., and Szentágothai, J. (1967). The Cerebellum as a Neuronal Machine (Heidelberg: Springer).

Galarreta, M., and Hestrin, S. (2001). Electrical synapses between GABA-releasing interneurons. Nat. Rev. Neurosci. *2*, 425–433.

Gao, W., Chen, G., Reinert, K.C., and Ebner, T.J. (2006). Cerebellar cortical molecular layer inhibition is organized in parasagittal zones. J. Neurosci. *26*, 8377–8387.

Hatton, G.I. (1998). Synaptic modulation of neuronal coupling. Cell Biol. Int. *22*, 765–780.

Häusser, M., and Clark, B.A. (1997). Tonic synaptic inhibition modulates neuronal output pattern and spatiotemporal synaptic integration. Neuron *19*, 665–678.

Heiney, S.A., Kim, J., Augustine, G.J., and Medina, J.F. (2014). Precise control of movement kinematics by optogenetic inhibition of Purkinje cell activity. J. Neurosci. *34*, 2321–2330.

Helbig, I., Sammler, E., Eliava, M., Bolshakov, A.P., Rozov, A., Bruzzone, R., Monyer, H., and Hormuzdi, S.G. (2010). In vivo evidence for the involvement of the carboxy terminal domain in assembling connexin 36 at the electrical synapse. Mol. Cell. Neurosci. *45*, 47–58.

Hormuzdi, S.G., Filippov, M.A., Mitropoulou, G., Monyer, H., and Bruzzone, R. (2004). Electrical synapses: a dynamic signaling system that shapes the activity of neuronal networks. Biochim. Biophys. Acta *1662*, 113–137.

King, J.S., Chen, Y.F., and Bishop, G.A. (1993). An analysis of HRP-filled basket cell axons in the cat's cerebellum. II. Axonal distribution. Anat. Embryol. (Berl.) *188*, 299–305.

Korbo, L., Andersen, B.B., Ladefoged, O., and Møller, A. (1993). Total numbers of various cell types in rat cerebellar cortex estimated using an unbiased stereological method. Brain Res. *609*, 262–268.

Lee, S., Yoon, B.E., Berglund, K., Oh, S.J., Park, H., Shin, H.S., Augustine, G.J., and Lee, C.J. (2010). Channel-mediated tonic GABA release from glia. Science *330*, 790–796.

Long, M.A., Landisman, C.E., and Connors, B.W. (2004). Small clusters of electrically coupled neurons generate synchronous rhythms in the thalamic reticular nucleus. J. Neurosci. *24*, 341–349.

Mann-Metzer, P., and Yarom, Y. (1999). Electrotonic coupling interacts with intrinsic properties to generate synchronized activity in cerebellar networks of inhibitory interneurons. J. Neurosci. *19*, 3298–3306.

McCracken, C.B., and Roberts, D.C. (2006). Neuronal gap junctions: expression, function, and implications for behavior. Int. Rev. Neurobiol. *73*, 125–151.

Medina, J.F., and Mauk, M.D. (2000). Computer simulation of cerebellar information processing. Nat. Neurosci. Suppl. *3*, 1205–1211.

Mittmann, W., Koch, U., and Häusser, M. (2005). Feed-forward inhibition shapes the spike output of cerebellar Purkinje cells. J. Physiol. *563*, 369–378.

Palay, S.L., and Chan-Palay, V. (1974). Cerebellar Cortex; Cytology and Organization (Berlin: Springer).

Pan, F., Mills, S.L., and Massey, S.C. (2007). Screening of gap junction antagonists on dye coupling in the rabbit retina. Vis. Neurosci. *24*, 609–618.

Park, S.M., Tara, E., and Khodakhah, K. (2012). Efficient generation of reciprocal signals by inhibition. J. Neurophysiol. *107*, 2453–2462.

Petreanu, L., Huber, D., Sobczyk, A., and Svoboda, K. (2007). Channelrhodopsin-2-assisted circuit mapping of long-range callosal projections. Nat. Neurosci. *10*, 663–668.

Pouzat, C., and Hestrin, S. (1997). Developmental regulation of basket/stellate cell—>Purkinje cell synapses in the cerebellum. J. Neurosci. *17*, 9104–9112.

Rela, L., and Szczupak, L. (2004). Gap junctions: their importance for the dynamics of neural circuits. Mol. Neurobiol. *30*, 341–357.

Rickgauer, J.P., and Tank, D.W. (2009). Two-photon excitation of channelrhodopsin-2 at saturation. Proc. Natl. Acad. Sci. USA *106*, 15025–15030.

Rieubland, S., Roth, A., and Häusser, M. (2014). Structured connectivity in cerebellar inhibitory networks. Neuron *81*, 913–929.

Santamaria, F., Tripp, P.G., and Bower, J.M. (2007). Feedforward inhibition controls the spread of granule cell-induced Purkinje cell activity in the cerebellar cortex. J. Neurophysiol. *97*, 248–263.

Schoenenberger, P., Grunditz, A., Rose, T., and Oertner, T.G. (2008). Optimizing the spatial resolution of Channelrhodopsin-2 activation. Brain Cell Biol. *36*, 119–127.

Somogyi, P., and Hámori, J. (1976). A quantitative electron microscopic study of the Purkinje cell axon initial segment. Neuroscience *1*, 361–365.

Sotelo, C., and Llinás, R. (1972). Specialized membrane junctions between neurons in the vertebrate cerebellar cortex. J. Cell Biol. *53*, 271–289.

Sultan, F., and Bower, J.M. (1998). Quantitative Golgi study of the rat cerebellar molecular layer interneurons using principal component analysis. J. Comp. Neurol. *393*, 353–373.

Tovar, K.R., Maher, B.J., and Westbrook, G.L. (2009). Direct actions of carbenoxolone on synaptic transmission and neuronal membrane properties. J. Neurophysiol. *102*, 974–978.

Vervaeke, K., Lorincz, A., Nusser, Z., and Silver, R.A. (2012). Gap junctions compensate for sublinear dendritic integration in an inhibitory network. Science *335*, 1624–1628.

Vincent, P., and Marty, A. (1996). Fluctuations of inhibitory postsynaptic currents in Purkinje cells from rat cerebellar slices. J. Physiol. *494*, 183–199.

Vincent, P., Armstrong, C.M., and Marty, A. (1992). Inhibitory synaptic currents in rat cerebellar Purkinje cells: modulation by postsynaptic depolarization. J. Physiol. *456*, 453–471.

Wang, H., Peca, J., Matsuzaki, M., Matsuzaki, K., Noguchi, J., Qiu, L., Wang, D., Zhang, F., Boyden, E., Deisseroth, K., et al. (2007). High-speed mapping of synaptic connectivity using photostimulation in Channelrhodopsin-2 transgenic mice. Proc. Natl. Acad. Sci. USA *104*, 8143–8148.

Zhao, S., Ting, J.T., Atallah, H.E., Qiu, L., Tan, J., Gloss, B., Augustine, G.J., Deisseroth, K., Luo, M., Graybiel, A.M., and Feng, G. (2011). Cell type-specific channelrhodopsin-2 transgenic mice for optogenetic dissection of neural circuitry function. Nat. Methods *8*, 745–752.